

Section II – Rhodes Workshop 2004

Integrated passive seismic acquisition and methodology. Case Studies

Nikos Martakis^{1*}, Sotiris Kapotas¹ and G-Akis Tselentis²

¹Landtech Enterprises S.A., 32 Kifissias Ave. Maroussi, 15125 Athens, Greece, ²University of Patras, Seismological Laboratory, Patras, Greece

Received December 2004, revision accepted May 2006

INTRODUCTION

Passive seismic uses natural microseismicity as seismic sources and stand-alone receivers (seismographs), which are laid out on the surface of the target area in such a way that they can produce results with maximum achievable resolution. Consequently, the passive seismic methodology is characterized by three main advantages over conventional seismic methodologies: it is cost effective, it is environmentally friendly and it is easily applicable, even in areas with the most difficult terrain.

The procedure of a passive seismic project can be divided into four basic steps: (a) a preacquisition (feasibility) study (b) acquisition and data analysis (assuming the presence of suitable natural seismicity) (c) an inversion process and (d) quality control (QC) of the results. A detailed description of these steps is presented here.

PRE-ACQUISITION (FEASIBILITY) STUDY

A passive seismic project depends mainly on the microearthquake activity in the study area. The first step is to collect all available information about the seismicity in the area, from the literature and from national and international seismological databases. With these data and using the well-known Gutenberg–Richter magnitude–frequency relationship (equation 1), we can then make an approximate estimation of the number of microearthquakes over a period of time:

$$\log N = a - bM, \quad (1)$$

where N is the number of earthquakes with magnitude equal to or greater than the magnitude M in a specific period of

time and space. The constants a and b can be calculated from known seismological data in the area of interest.

Furthermore, we can depict a clear image of the distribution of seismic events. The disadvantage of these seismological data sets is that they are derived from sparse seismic networks, so it is possible to lose some significant information regarding the very low magnitude seismic activity (we can only approach and estimate it from a theoretical point of view). To overcome this difficulty, we can install a network of 5–10 seismic stations for a period of 1–2 months, in order to ensure a sufficient number of events over the acquisition period and to improve the quality of the information we acquire about the study area.

The feasibility study is imperative for the acquisition design of a passive seismic project. Taking into account all the resulting information, both theoretical and experimental, we are able to estimate not only the appropriate acquisition time and the geometry of the seismic network, but also the expected resolution of the final data. Therefore, our approach is to run some synthetic tests using the procedure described below.

Firstly, we construct a synthetic seismicity pattern, which is based on geological and seismological information over an appropriate time period, using a seismic network distribution based on the objectives of the project. The next step (forward modelling) is to calculate the P- and S-wave traveltimes from sources to receivers, using a known (if possible) 3D synthetic velocity model that is compatible with previous studies that have taken place in the region. In the absence of such a model, the most common test to apply is the checkerboard one. The last part of a feasibility test is the inversion process, which starts with a 1D layered velocity model and the calculated traveltimes. The main target is the best possible reconstruction of the known 3D model.

*E-mail: nmartakis@landtechsa.com

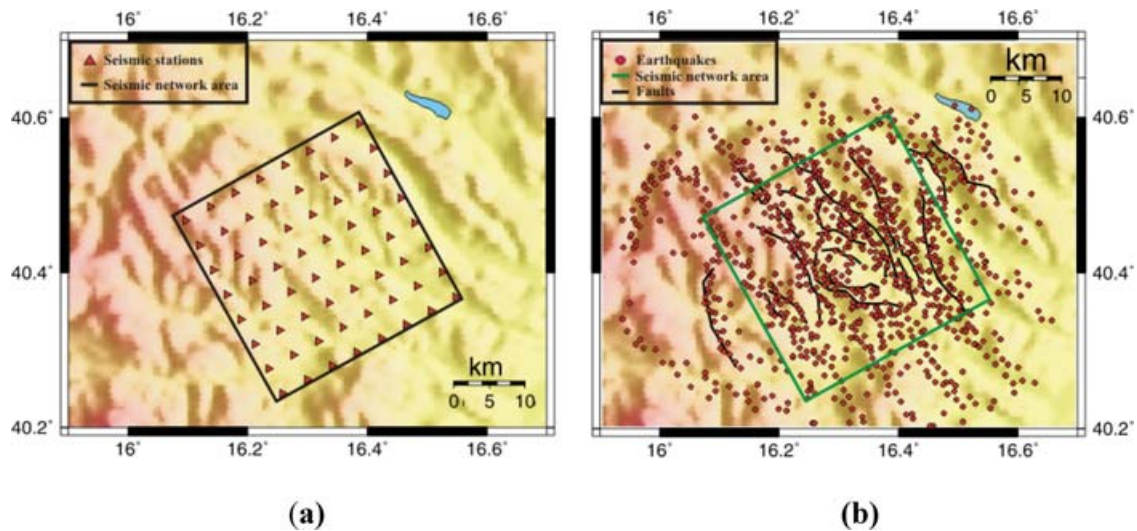


Figure 1 (a) Microseismic network design for 64 stations and (b) synthetic seismicity pattern for a feasibility study.

The comparison between the initial synthetic velocity model and the calculated one, along with resolution functions like the number of rays per cell (the hit count), the derivative weighted sum (DWS) and the resolution diagonal elements (RDE), can yield information about the expected accuracy of the model and the possible undersampled areas. All these functions will indicate the proper network geometry and indicate modifications if needed.

It is expected that possible undersampled areas could be found in the shallower parts of the model, due to the verticality of seismic rays reaching a receiver. The shallow-structure resolution can be considerably improved by increasing the number of stations or with periodic redeployments of the network in order to cover 'white' spots.

In the following example, we present a feasibility synthetic inversion test based on a homogeneous local seismicity of 1000 events and an array of 64 stations covering a target region of 900 km² (Fig. 1).

The initial (known) synthetic 3D model is a 1D layered velocity model with superimposed velocity anomalies of the order of $\pm 5\%$ of the layer velocity at the corresponding depth. Following the procedure described above, with our inversion scheme we calculated a 3D velocity model starting with the initial 1D model.

Figure 2 shows a plan view of the results of a checkerboard test at 3.2 km depth. The background layered model has been removed and only the velocity anomalies are visible to make the results of the checkerboard test clearer. It is obvious that the reconstruction of the model is extremely accurate, espe-

cially in the central part of the study area. The red line in Fig. 2 is related to the cross-sections presented in Fig. 3.

Figure 3 shows cross-sections comparing the calculated and synthetic 3D velocity models. In the top row, the absolute P-wave velocities V_P are compared. The two cross-sections in the middle row focus exclusively on a comparison of the superimposed velocity anomalies; the cross-section at the bottom indicates the ray coverage of this part of the model.

The comparison reveals that the reconstruction of the model is very successful, especially at depths greater than 1.5 km. It is also obvious from the ray coverage that there are undersampled areas in the shallower part of the model, even though the grid size is greater than in the deeper part where the ray coverage is almost homogeneous (Fig. 4)

ACQUISITION AND DATA ANALYSIS

If the feasibility study shows that passive seismic can successfully obtain the desired results, the next phase of a project is the acquisition and collection of seismological data and analysis. The basic steps of the acquisition set-up are the following:

- definition of monitoring (seismic network) area;
- selection of monitoring sites;
- instrument deployment;
- noise tests;
- definition of recording parameters.

The network area is selected according to the target location of the project and the expected seismicity. At each monitoring site, easily accessible and low-noise locations have to be

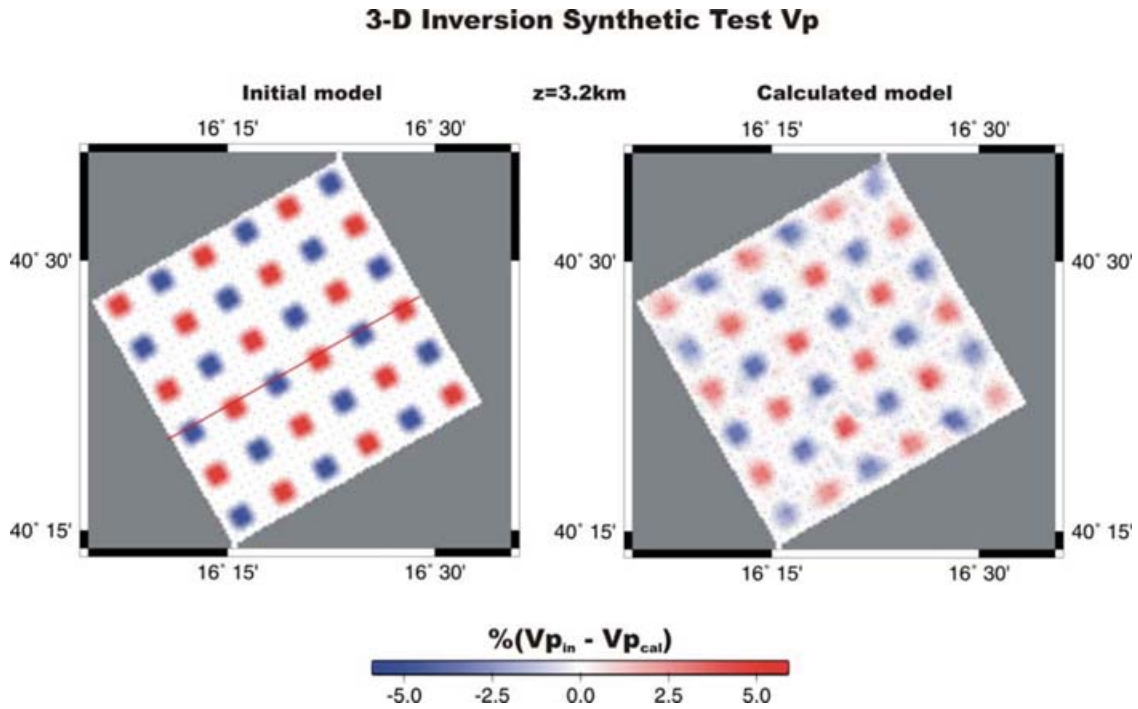


Figure 2 Plan view of a checkerboard test. Initial synthetic $\pm 10\%$ velocity anomalies used to generate synthetic traveltimes (left); reconstruction of velocity anomalies after inversion using the source–receiver geometry described in Figure 1 and a 1D velocity model as initial model (right). The red line refers to Figure 3.

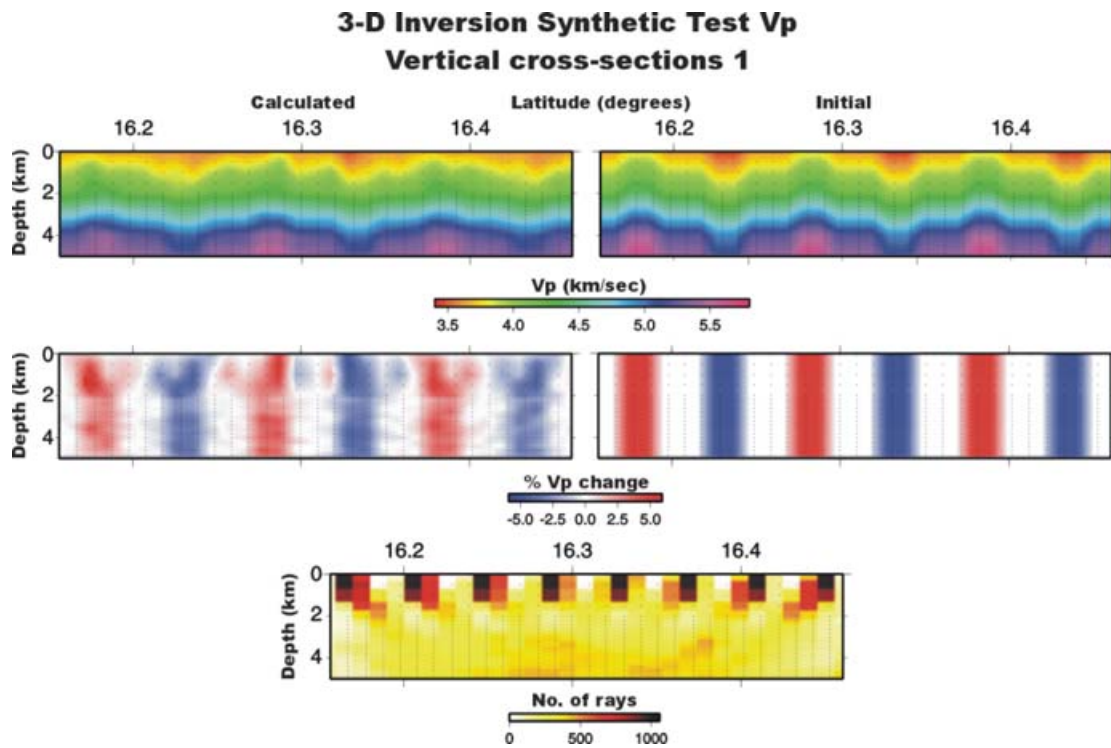


Figure 3 Cross-section showing the results of a feasibility study along the red line (Figure 2). Comparison of the velocities of the initial synthetic and the calculated models (top); comparison of velocity anomalies (centre); ray coverage (bottom).

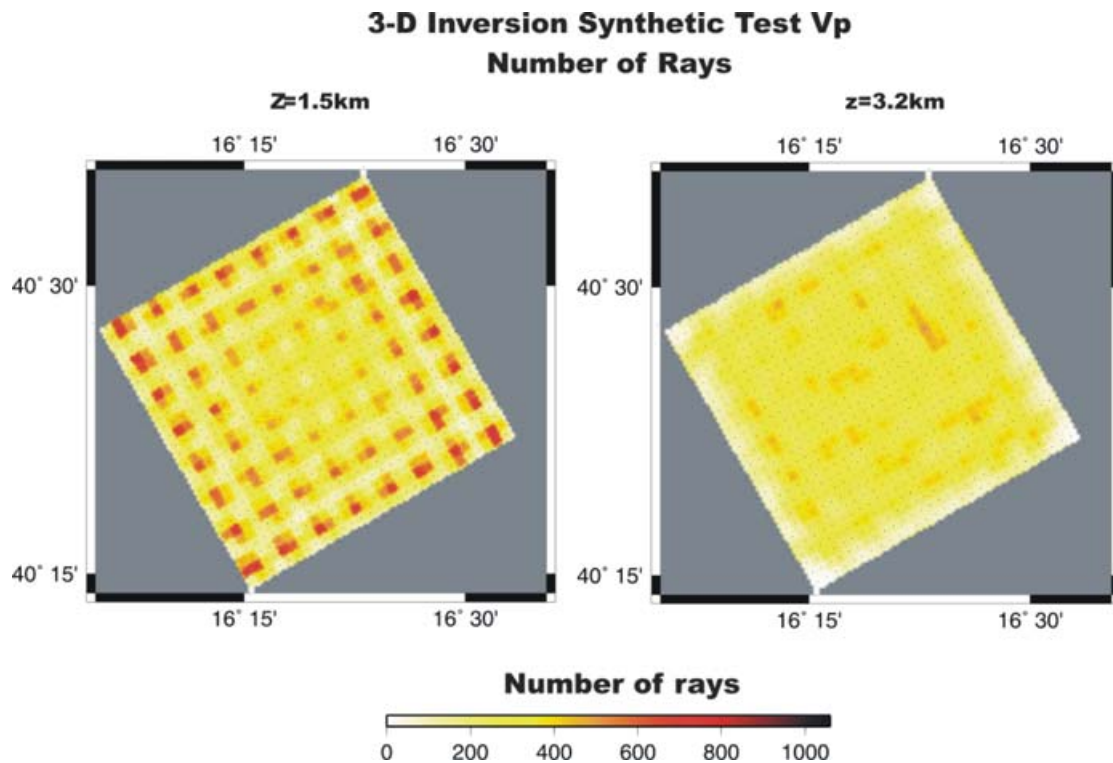


Figure 4 Plan view of ray coverage at 1.5 km depth (left) and at 3.2 km depth (right).

found, where possible. Furthermore, it is advisable to avoid alluvial deposits in order to obtain better quality of the recorded signal and to increase the density of the network in areas of interest.

The instruments used for the acquisition are seismographs and seismometers. Seismometers are often placed in shallow boreholes 2–15 m deep, in order to achieve a better coupling and to reduce any environmental noise. The seismometer is connected to the seismograph, which is placed at the surface in a small vault or similar unit so as to achieve maximum safety and weather protection. Both seismograph and seismometer can operate under difficult weather conditions.

We use Earthdata digital 24-bit seismographs with a variable sampling rate from 1 to 1000 Hz and LandTech three-component seismometers with a frequency bandwidth from 0.2 to 106 Hz. Each station is also equipped with a 12 V battery supply. If there is no power supply in the area of a seismic station, the batteries are charged by solar panels or by specially designed wind generators. Due to low power consumption, a seismic station can operate continuously for more than two weeks using a 12 V battery. In order to avoid operational problems that may occur within the network, the field

crews perform thorough inspections of all the stations every three or four days. Seismic stations are time synchronized via GPS. Usually, all seismographs of the network can transmit a state-of-health code via telemetry to inform the network operator of problems that might possibly occur, such as high noise levels or low battery levels.

The most common recording pattern is in continuous mode and the sampling rate is 100 or 200 samples per second. The recorded data are stored in 80 GB hard disk drives and can be transmitted to the data centre via telemetry (e.g. GSM, GPRS, satellite, FM) or manually by exchanging the hard disks periodically.

Data analysis includes seismic event separation, phase picking and hypocentre location. For the separation and the phase picking, we use the SISMWIN software package (Xanalatos and Tselentis 1997) and for the calculation of the initial locations, we use the HYPO71PC program (Lee and Lahr 1972), the HYPOINVERSE-2000 program (Klein 2002) or the HYPODD program (Waldhauser 2001).

The separation of the most accurately located seismic events from the whole data set that will be employed in the inversion process is the last step of the data analysis.

INVERSION PROCEDURE AND QUALITY CONTROL

The inversion procedure of a 3D passive seismic tomography can be described by dividing it into three main steps. The first one is the estimation of the best-fitting 1D initial model in parallel with the optimization of the hypocentre locations. The second is the 3D model construction and the third is related to the quality control of the results.

Minimum 1D velocity model estimation

The results and the reliability of the 3D tomographic inversion, which is solved as a linear approximation of a non-linear function, depend on the initial reference model. The target is to derive an appropriate initial 1D velocity model, with the corresponding station corrections, that minimizes the rms error of hypocentre locations. This procedure is an iterative joint hypocentre – velocity inversion.

Apart from the minimization of the error in the hypocentre locations, tests have to be performed in order to check the quality of the 1D inversion results, such as the convergence of different starting 1D velocity models, the recovery of hypocentre locations after random shifting and the comparison of station delays with the crustal structure (Haslinger 1998).

3D velocity model estimation

The aim of passive seismic tomographic inversion is the estimation of a 3D velocity model and the corresponding hypocentre parameters, having as known parameters only the arrival times of the P- and S-waves at the seismic stations, a first estimation of the hypocentre locations and the positions of the seismic stations (all with some uncertainty).

According to ray theory, the traveltimes T_{ij} of a seismic wave from hypocentre i to receiver j can be described by the integral equation,

$$T_{ij} = \int_{\text{source}}^{\text{receiver}} u \, ds, \quad (2)$$

where u is the slowness field and ds is a ray segment along the raypath. The seismic-wave arrival times τ_{ij} can be written as

$$\tau_{ij} = \tau_i + T_{ij}^s(x_i, y_i, z_i, u(s), x, y, z), \quad (3)$$

where τ_i is the time of origin of the i th earthquake, x_i, y_i, z_i are the coordinates of the source and x, y, z are the coordinates of the receivers.

The arrival-time residuals $r_{ij} = \tau_{ij}^{\text{obs}} - \tau_{ij}^{\text{cal}}$ can be written as a linear system of equations:

$$r_{ij} = \sum_{k=1}^3 \frac{\partial T_{ij}}{\partial x_k} \Delta x_k + \Delta \tau_i + \sum_{l=1}^L \frac{\partial T_{ij}}{\partial m_l} \Delta m_l, \quad (4)$$

where Δx_k and Δm_l are the perturbations to the hypocentre parameters and the velocity perturbations, respectively. The partial derivatives in equation (4) can be calculated, given the velocity model and the raypath from the earthquake to the seismic station. The partial derivatives with respect to the hypocentre parameters are given by the equation (Lee and Stewart 1981; Thurber 1983),

$$\frac{\partial T_{ij}}{\partial x_k} = -\frac{1}{V} \left(\frac{dx_k}{ds} \right)_{\text{source}}. \quad (5)$$

The partial derivatives with respect to the velocity model parameters are calculated as approximations of the path integrals given by the equation (Thurber 1983),

$$\frac{\partial T_{ij}}{\partial m_l} = \int_{\text{source}}^{\text{receiver}} - \left\{ \frac{1}{V(x, y, z)} \right\}^2 \frac{\partial V(x, y, z)}{\partial m_l} ds. \quad (6)$$

In equation (5), the velocity $V(x, y, z)$ and its partial derivative with respect to a model parameter can be calculated by an interpolation scheme.

The minimization of the arrival-time residuals is an iterative procedure including the solution of the forward and inverse problem during each step. The linearized inversion can be written in matrix notation as

$$\Delta \mathbf{d} = \mathbf{G} \Delta \mathbf{m}, \quad (7)$$

where \mathbf{G} is the Jacobian matrix that contains all the partial derivatives in equation (3), $\Delta \mathbf{d}$ denotes the residuals and $\Delta \mathbf{m}$ denotes the perturbations of the model parameters. In practice, the problem of passive tomography is usually underdetermined or mixed determined. For this reason, we apply the damped least-squares method:

$$\Delta \mathbf{m} = \mathbf{G}^T \mathbf{G} + \varepsilon^2 \mathbf{I}^{-1} \mathbf{G}^T \Delta \mathbf{d}, \quad (8)$$

where ε^2 is the damping factor.

The tomographic inversion presented in this study is based on an optimized version of the SIMULPS12 software (Evans *et al.* 1994 revised version of the SIMUL3M code by Thurber 1983). The procedure adopts the SVD algorithm for the solution of the inverse problem, incorporating a parameter separation scheme (velocity and hypocentre parameters) in order to reduce the computational cost of the process (Thurber 1983). The parametrization of the problem is based on the 3D grid

of nodes technique. The forward problem is solved with two different and well-tested ray-tracing algorithms.

Quality control

Checking the resolution and reliability of the inversion results is regarded as the final basic step of the inversion procedure. The procedure followed is the same as that adopted in the feasibility study, but in this case the recorded seismicity is used instead of the synthetic seismicity.

Many techniques have been proposed in previous studies. The most common methods are: the calculation of the hit count; DWS (derivative weighted sum); RDE (resolution diagonal elements). The first method is the summation of rays which pass through the region of influence of a model parameter. The DWS provides us with a more reliable estimation of the sampling of the study area because it sums up all the ray segments in the region of influence of one velocity parameter, weighting them according to the distance from it. The RDE (equation 9) are the diagonal elements of the resolution matrix \mathbf{R} , which is described by equation (8). These equations are the result of the SVD solution of the equation (8) (Lanczos 1961):

$$\mathbf{R} = \mathbf{V} \left(\frac{\Lambda^2}{\Lambda^2 + \varepsilon^2 \mathbf{I}} \right) \mathbf{V}^T, \quad (9)$$

$$\mathbf{R}_{\text{diag}} = \left(\frac{\Lambda^2}{\Lambda^2 + \varepsilon^2 \mathbf{I}} \right), \quad (10)$$

where Λ is the matrix that contains the singular values.

The full resolution matrix offers important information about the quality of the inversion results. Each row of matrix \mathbf{R} describes the dependence of one model parameter on all the other parameters of the model. Although the resolution matrix is a very significant way of checking the quality of tomography results, it is computationally very consuming to interpret it. Therefore, instead, the RDE are used as the most common parameters to assess solution quality.

Another important quality control parameter is the spread function (Toomey and Fougler 1989; Michelini and McEvilly 1991), which provides information about how far the solution at one model parameter is affected. The spread function for the j th model parameter is given by the equation,

$$S_j = \log \left(|s_j|^{-1} \sum_{k=1}^m \left(\frac{s_{kj}}{s_j} \right)^2 D_{jk} \right). \quad (11)$$

All the above-mentioned parameters for the estimation of the quality of the inverse problem solution can provide useful

information. However, some disadvantages have to be considered. The hit count is a crude measure of the sampling of the study volume because it does not use any information about the ray-segment length in the vicinity of a model parameter or the observation weight. The DWS depends on the ray-segment length. The RDE and the spread depend on the grid spacing and the damping value used in the inversion process (Eberhart-Phillips 1986; Toomey and Fougler 1989).

The most appropriate method of estimating the reliability of the tomography results is the synthetic sensitivity test. The advantage of this procedure is that it can give information about the effects of the model grid spacing and the distribution of the data. In addition, it is able to estimate how close the calculated model parameters are to the initial absolute values. In most cases, the checkerboard test is used, following the technique described for the feasibility study.

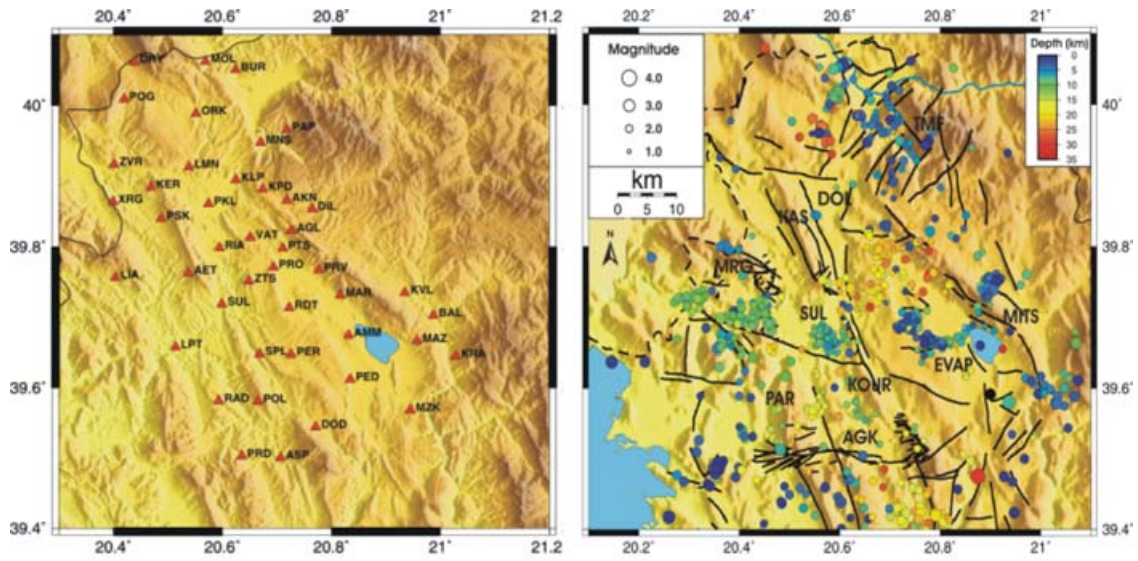
A combination of the above-mentioned methods can provide significant information about the reliability of the resulting models and can be very useful in identifying possible artefacts, consequently avoiding misinterpretations.

CASE STUDIES

The results of the methodology described can be seen in the following case studies. The first case study is from a hydrocarbon exploration project in NW Greece. The second is a small-scale tomography study that took place in western Greece (the Rio-Antirio pass) and its scope was the feasibility of a subsea tunnel construction in the area. Below, only a brief description of these case studies will be presented.

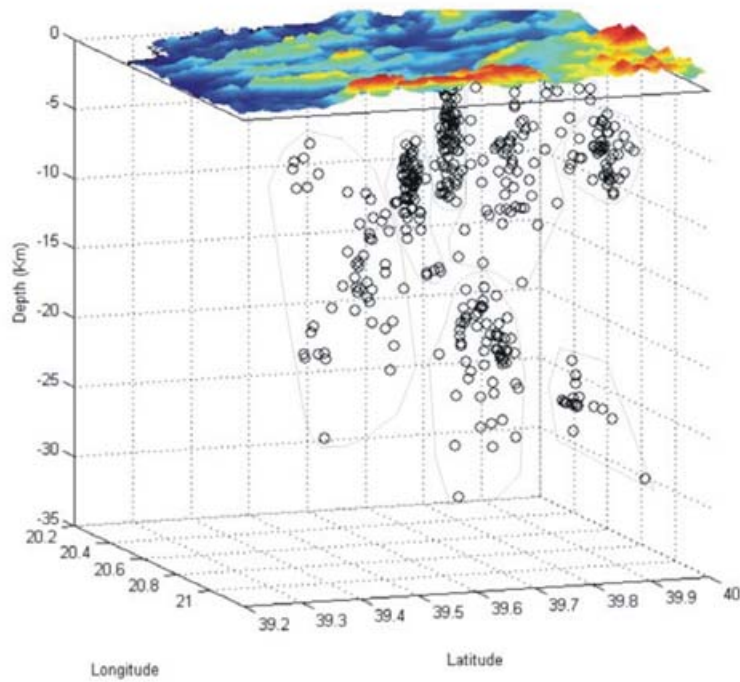
Case study I: Epirus (NW Greece)–hydrocarbon exploration

This project started in June 1998 and terminated 10 months later (Kapotas, Tselentis and Martakis 2003). The study area is located in a very complicated thrust-belt zone. The seismic network, which covered an area of about 3000 km², consisted of 40 stations. In the monitoring period more than 900 earthquakes were recorded and 450 located events were used for the tomographic inversion (Figs 5a,b). The hypocentre depths of the selected events range from 500 m down to 35 km but the majority of them are located in the shallower part of the study volume, between 500 m and 15 km (Fig. 5c). The 450 events satisfied the following criteria: they were located within the seismic network and they had at least 20 P- and S-wave arrivals, maximum rms residuals of 0.20 s and a location error of less than 1 km.



(a)

(b)



(c)

Figure 5 (a) Microseismic network for passive seismic survey in Epirus, NW Greece;(b) recorded seismicity during 10-month project. The black lines describe the most important known faults within the study area. (c) 3D view (from west) of distribution of microearthquakes.

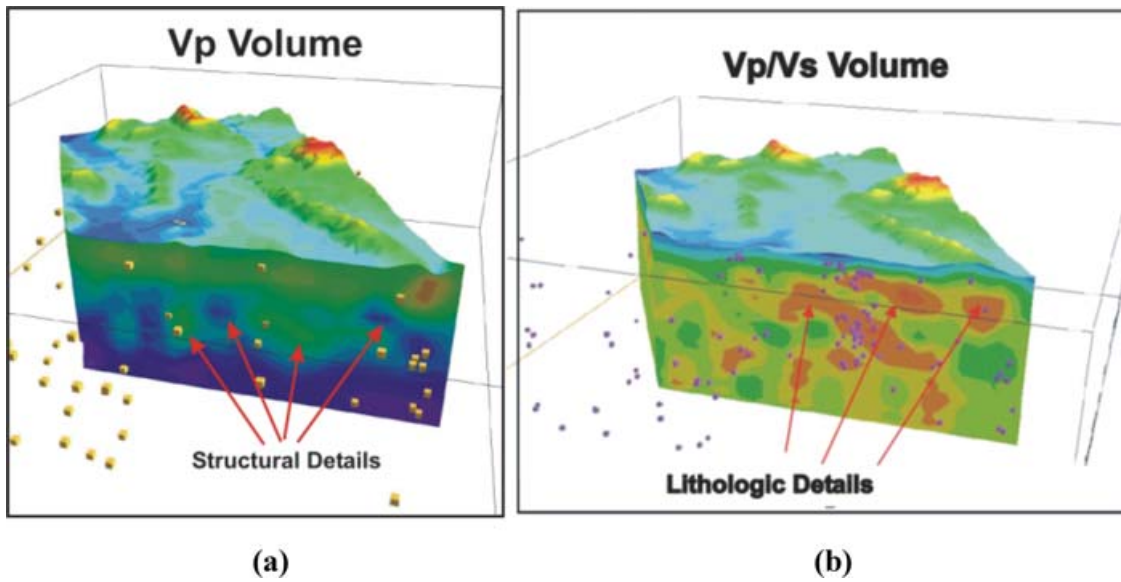


Figure 6 (a) P-wave velocity section showing structural details of the crust. Green is related to evaporite and blue to carbonate characteristic velocities. (b) V_p/V_s section showing lithological details. Brown indicates the existence of evaporite along thrust faults.

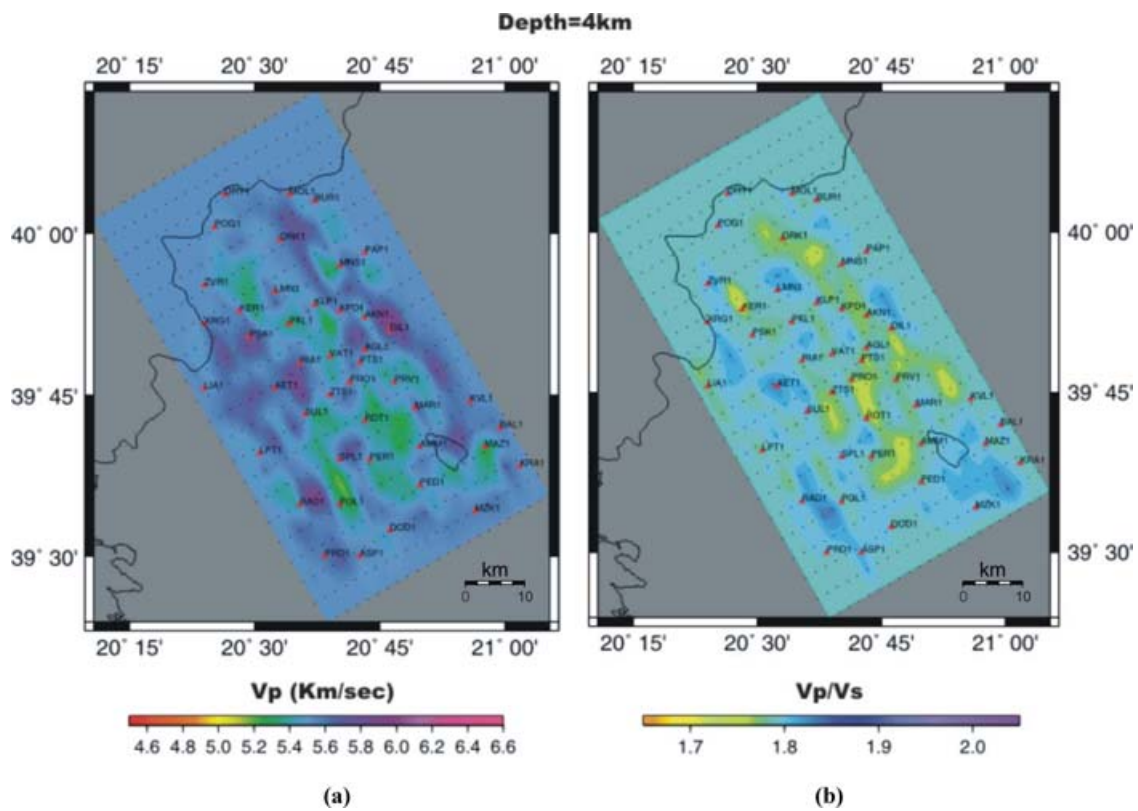


Figure 7 (a) Plane sections of P-wave velocity and (b) V_p/V_s ratio at 4 km depth.

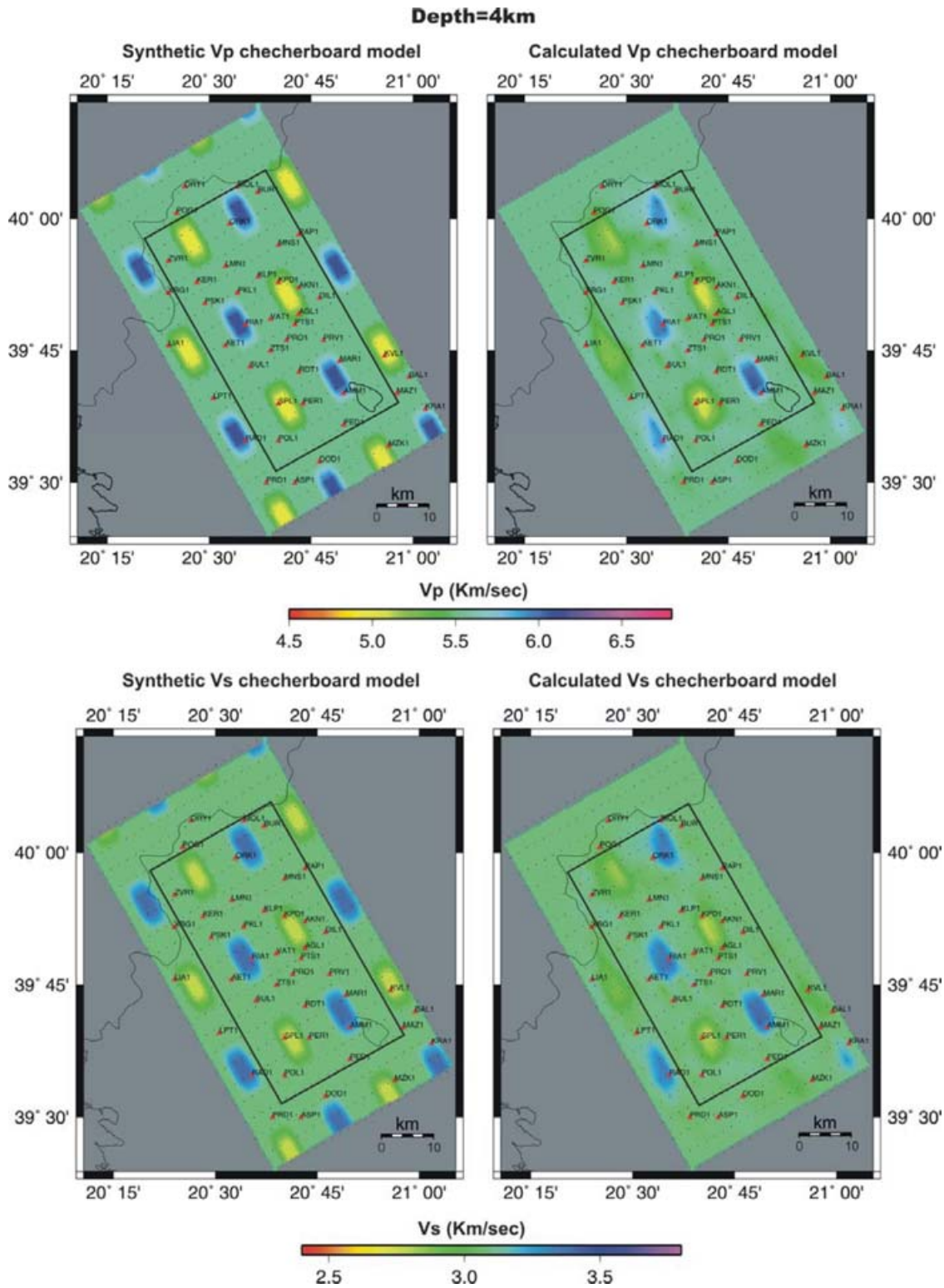


Figure 8 Checkerboard test for V_p model (top) and V_s model (bottom) at 4 km depth. The initial synthetic models are shown on the left and the reconstructed ones are on the right. The target area, which is the best resolved, is included within the black parallelogram.

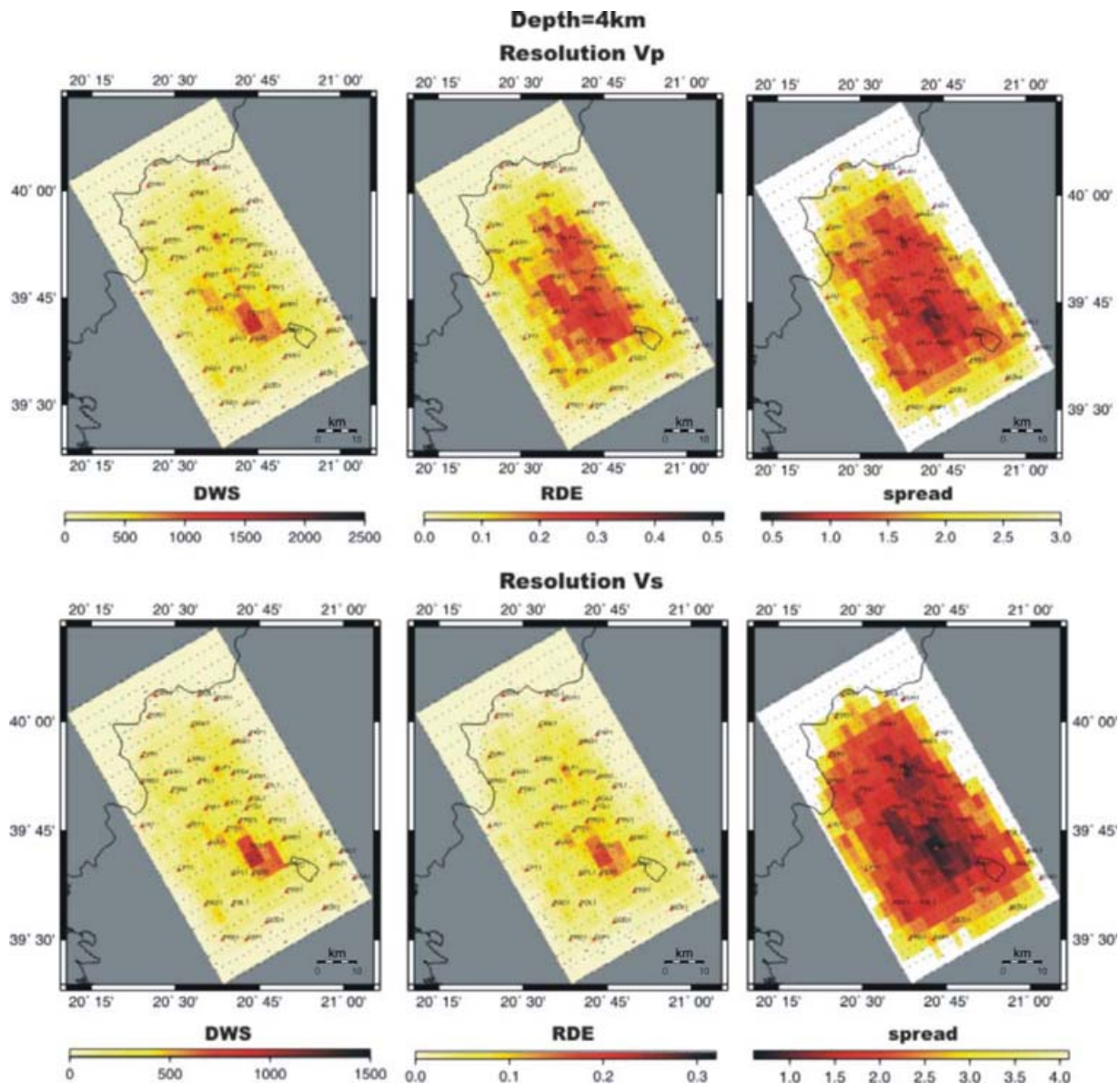


Figure 9 Description of resolution parameters at 4 km depth for V_p (top) and V_p/V_s (bottom).

The velocity model used by the Seismological Laboratory of Patras University for Western Greece (Melis and Tselentis 1998) was adopted as the initial model for the preliminary calculation of the microearthquake locations. The first step of the tomographic procedure was the estimation of the 1D minimum-velocity model. The average rms travelt ime residual after 1D inversion was 0.119 s.

The minimum 1D velocity model was used as the initial model for the joint hypocentre and velocity 3D inversion step. A 3D grid of nodes was used for the model parametrization.

The velocity values within each voxel were calculated using a linear spline interpolation scheme. The initial grid spacing was set at $2 \times 4 \times 1$ km for the whole study area. After five iterations, the final 3D V_p and V_p/V_s models were obtained with an average rms misfit of 0.076 s. The location error in the majority of the relocated events (based on the 3D models) was less than 500 m and that in the rms residuals was less than 0.08 s. A finer grid spacing ($1 \times 1 \times 0.5$ km) was tested in order to compare some specific features of the model around the area, where an oil-exploration

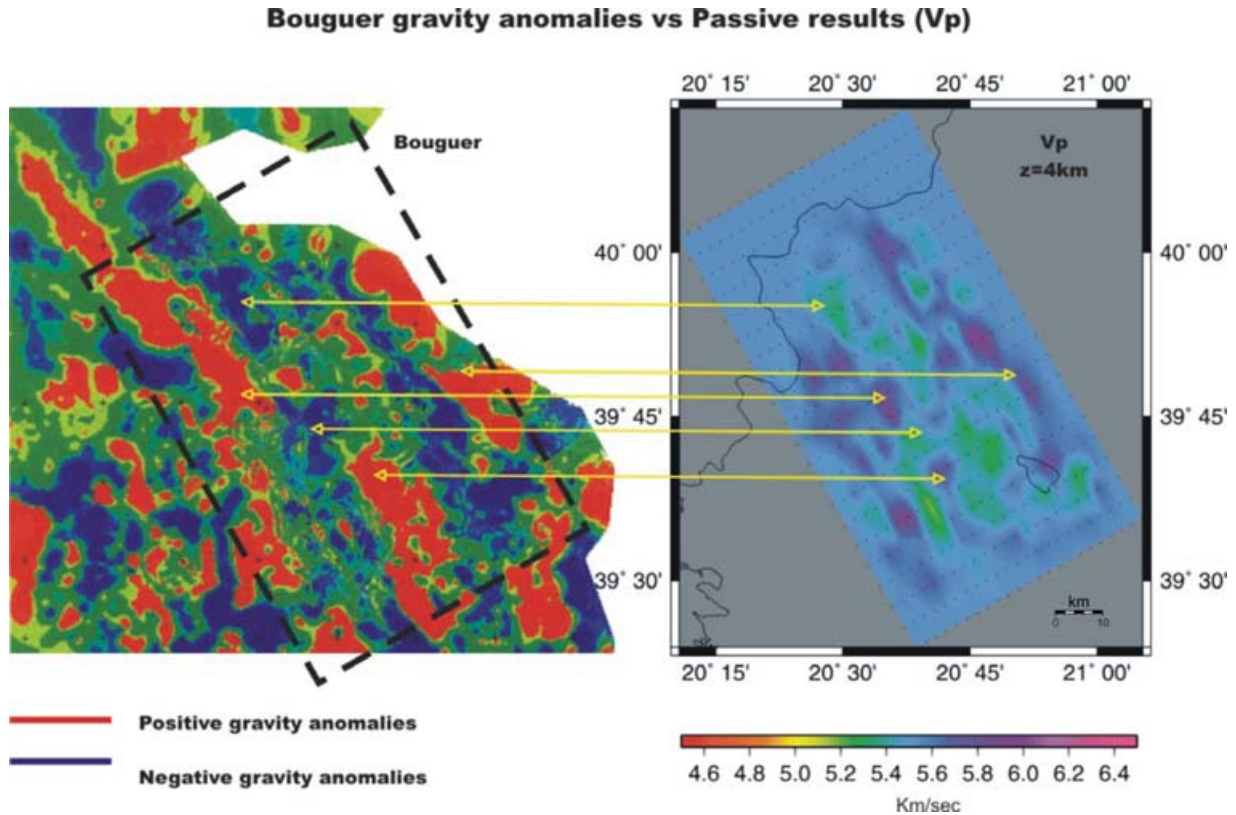


Figure 10 Comparison between Bouguer gravity and passive seismic results for V_p . Positive and negative gravity anomalies are related to high- and low-velocity values, respectively.

well was drilled, with the results from other geophysical data (i.e. VSP).

Figures 6(a,b) shows some characteristic sections of the resultant V_p and V_p/V_s models. In Fig. 6(a), the V_p section provides important structural details of the volume studied while the V_p/V_s section adds valuable lithological information. The interchange between evaporite (green: 5.0–5.4 km/s) and carbonate (blue: 5.6–6.0 km/s) structures due to overthrusting can be clearly seen in Fig. 6(a). The overthrust zone is described in detail by the V_p/V_s model (Fig. 6b). Areas characterized by low V_p/V_s values (brown: 1.65–1.75) correspond to evaporitic intrusions through carbonates (green: 1.78–1.85), following the thrust faults. High V_p/V_s values near the surface (blue: > 1.85) correspond to a karstified and saturated carbonate layer. The carbonate and evaporitic structures can be also seen in Figs 7(a,b), which describes the P-wave velocity and V_p/V_s distribution at 4 km depth.

Tomographic results make sense only if they are quantified by quality control. One of the QC tests we used is the checkerboard test. The starting 1D velocity model for the 3D inversion, with $\pm 10\%$ superimposed velocity anomalies, was

used as a synthetic model for the generation of the synthetic traveltimes. The reconstruction of $\pm 10\%$ synthetic velocity anomalies (V_p and V_s) at 4 km depth is shown in Fig. 8. RDE, DWS and spread values at 4 km depth provide additional information about the resolution (Fig. 9). Comparing Figs 8 and 9, we can observe which areas within the model are better resolved. It can be clearly seen that P-wave velocity anomalies are very well resolved within the target area where DWS values are greater than 250, RDE more than 0.15 and the spread less than 1.5. The results for V_s are almost the same but with relatively lower quality due to fewer S-wave data.

Another way to test the accuracy and quality of tomographic results is to compare them with the results from other geophysical methods. The fact that the passive seismic survey was a part of an oil-exploration project in Epirus gave us the opportunity to compare the results obtained from the passive seismic measurements with other methods and with VSP data from the well. The P-wave velocity obtained by passive seismic fits Bouguer gravity results very well (Fig. 10). An excellent fit between V_p and V_p/V_s results from passive seismic and VSP data is obvious (Figs 11a,b,c). It is very important

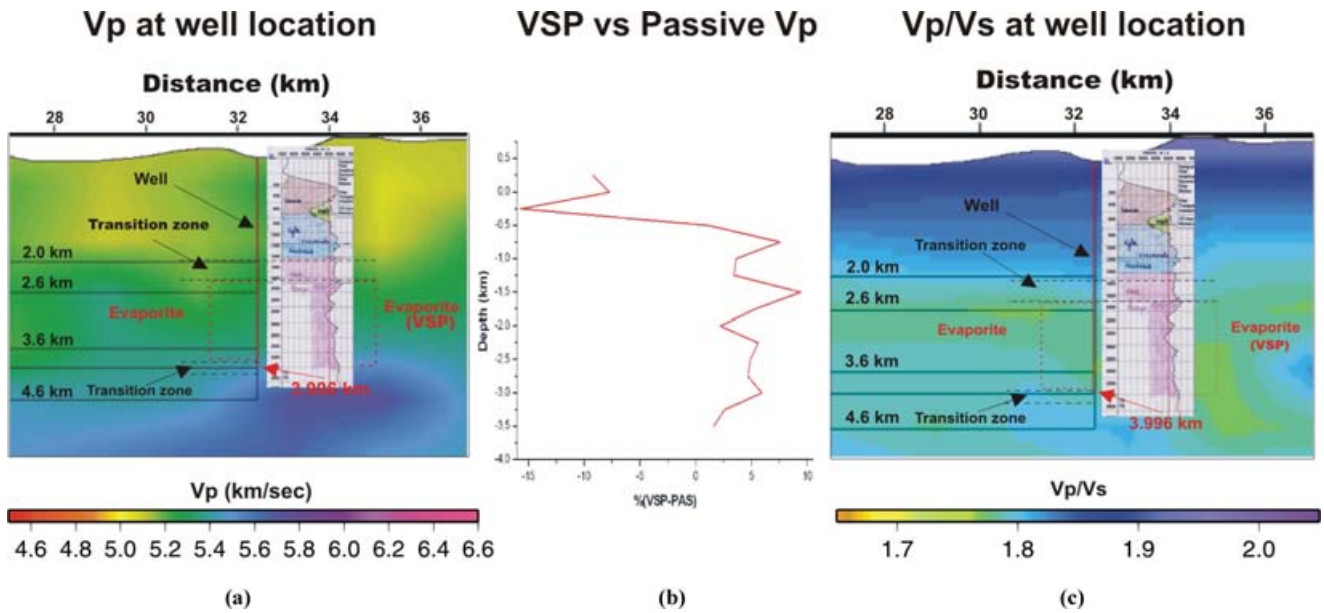


Figure 11 Comparison between passive seismic and VSP results. (a) VSP versus passive seismic at well location; (b) VSP versus passive seismic velocity values; (c) VSP versus V_p/V_s at well location.

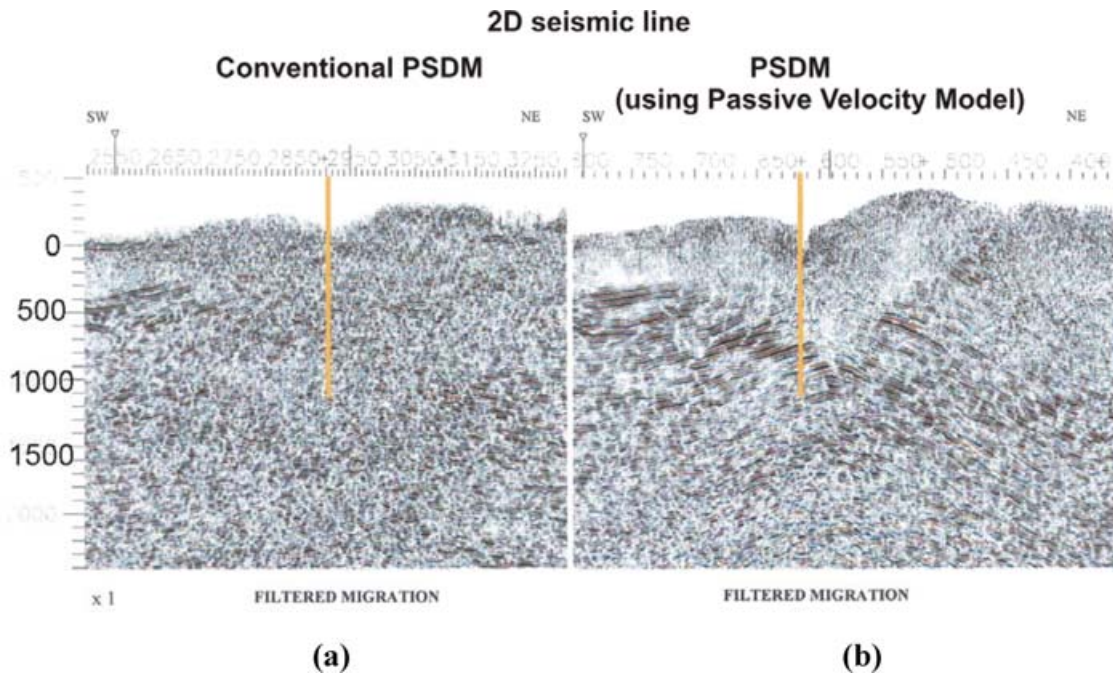
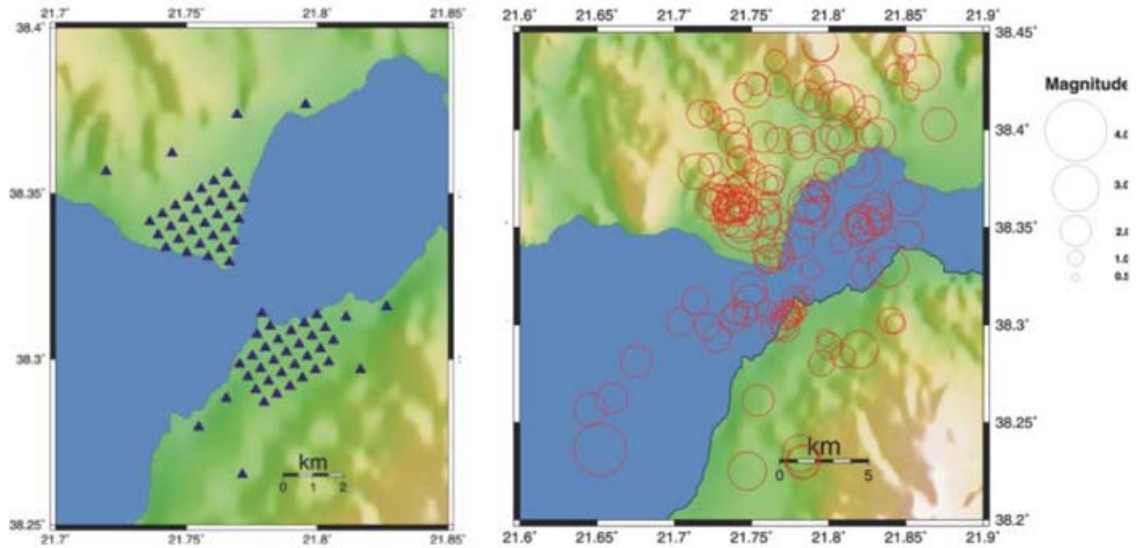


Figure 12 (a) 2D conventional PSDM seismic line; (b) 2D PSDM seismic line using passive seismic velocity model.

to mention that the V_p velocity difference between passive seismic and VSP at the well is less than 10% from 500 m below m.s.l down to 3.997 km (where drilling stopped because of high pressure). This difference is higher than 10% only in the part from the surface down to 500 m due to the vertical-

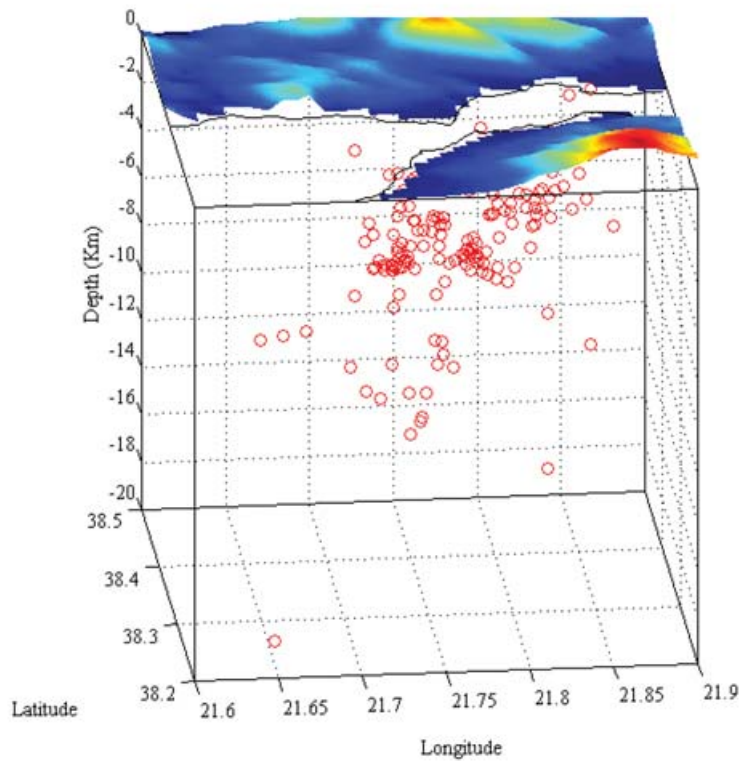
ity of rays near the surface which leads to poor ray coverage (Fig. 11b).

The final evidence of the success of the passive seismic survey in Epirus is that the V_p model was used for reprocessing very poor quality 2D conventional seismic data. The



(a)

(b)



(c)

Figure 13 (a) Microseismic network for a small-scale passive seismic project in the Rio-Antirio area, western Greece. (b) Recorded seismicity in the Rio-Antirio area during a 5-month period; (c) 3D view (from the south) of the distribution of seismic events.

comparison before and after PSDM using the passive seismic velocity model (Fig. 12) shows significant improvement and similarity to the V_P/V_S section at the well area (Fig. 11c).

Case study II: Rio-Antirio project (western Greece)

The tomographic survey at the Rio-Antirio pass finished in July 2004. The monitoring period was 5 months. More than

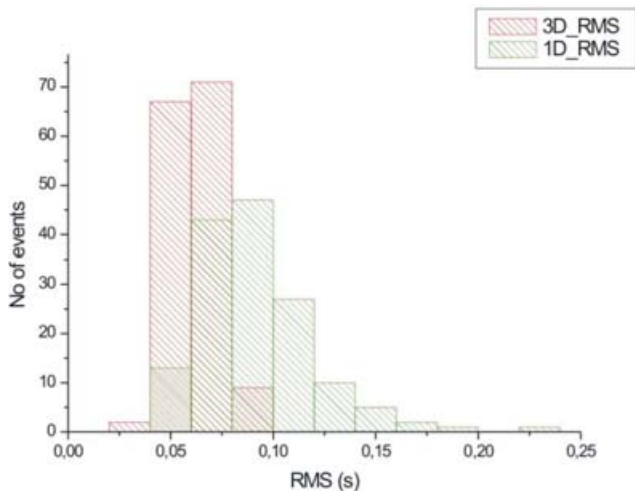


Figure 14 Rms distribution of seismic events for minimum 1D velocity model (green) and 3D velocity model (red).

200 microearthquakes were recorded and their hypocentre locations were initially computed, based on the 1D velocity model used by Seismological Laboratory of Patras University for Western Greece (Melis and Tselentis 1997). It was a small-scale project (less than 100 km²) and the seismic network consisted of 70 stations that covered the onshore part of the study area (Fig. 13a). Unfortunately, 4 OBS stations that were proposed in order to cover the offshore part were rejected, due to cost.

The objectives of the project were the estimation of the thickness of Quaternary and Neogene formations, the mapping of the basement, the identification of active faults and the seismicity distribution in the area of the Rio-Antirio pass. The estimation of the shallower earthquake locations was very important for the design of the submersible tunnel to be placed on the sea bottom. The maximum water depth in the area of interest was 65 m.

150 seismic events with an average of 59 P- and S-wave arrivals were selected for the tomographic inversion. The magnitude range was between -0.5 and 3.0 on the Richter scale, except for one earthquake that was located in the Antirio fault area, which had a magnitude 4.5 on the Richter scale. The hypocentre depths varied between 2 and 20 km, but most of the events were located between 2 and 12 km. The average rms residual for these events was 0.87 s after the minimum

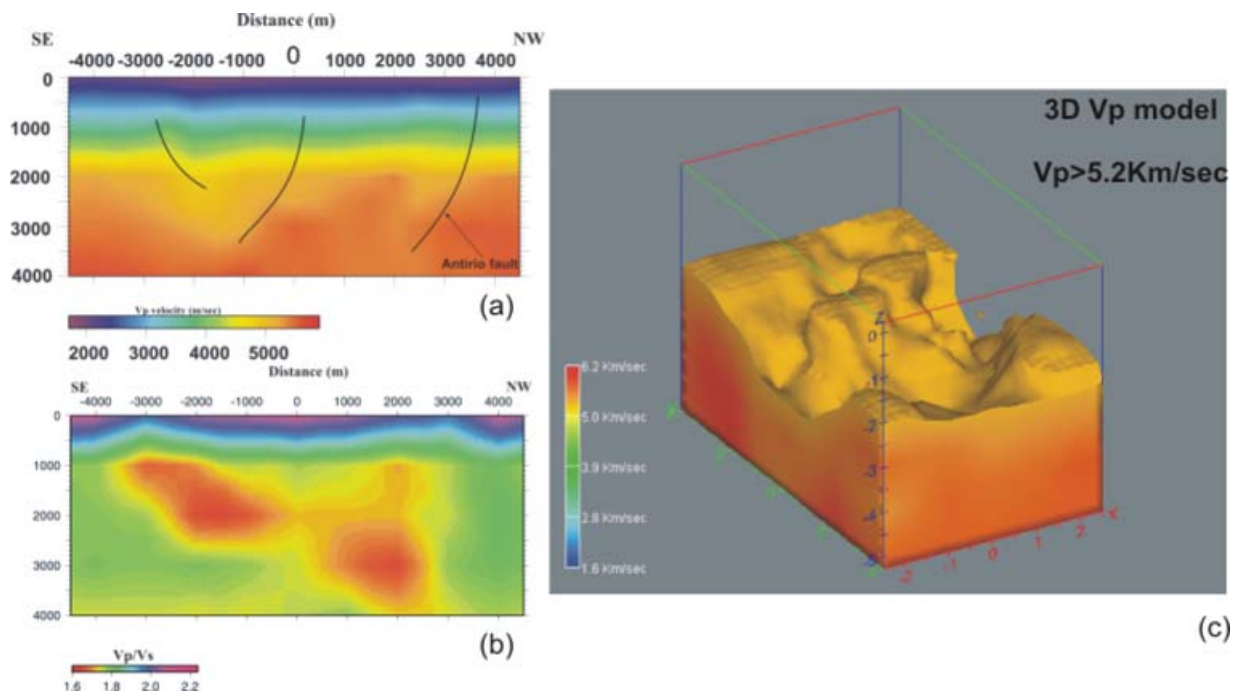


Figure 15 (a) Cross-section of V_P velocity model. The black lines are related to faults within the study area. (b) Cross-section of V_P/V_S model. (c) 3D view of the V_P velocity model showing structural details of the area.

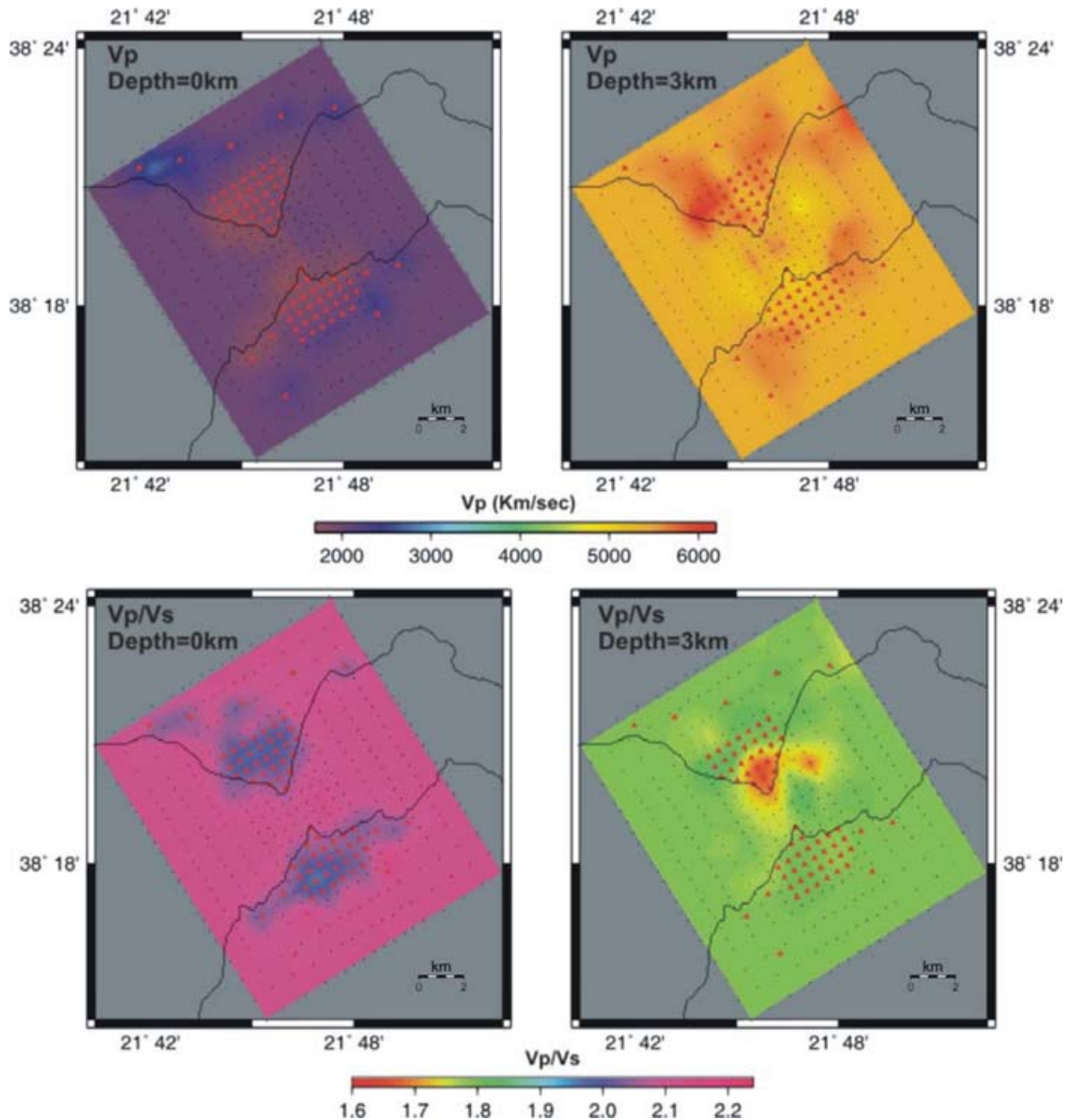


Figure 16 Plan view of V_P model (top) and V_P/V_S model (bottom) at 0 and 3 km depth.

1D velocity model inversion. The recorded seismicity distribution is shown in Figs 13(b,c).

In order to overcome the ray coverage problem in the offshore part of the study area, a graded 3D inversion scheme was adopted for the velocity model construction, due to the network gap. The first step of this procedure was the construction of a velocity model for the whole network area, using a grid of nodes with dimensions of $1 \times 1 \times 1$ km. The resultant 3D model was used as a starting model in the second step where we used a grid of nodes with dimensions $0.5 \times 0.5 \times 0.5$ km for the inversion, only in the target area. Further opti-

mization of the 3D model could have been possible in the land section of the target area where the spacing between stations was 500 m, but the lack of OBS stations in the sea section of the area could produce undesirable resolution inhomogeneity.

The average rms residual for the relocated seismic events, based on the final 3D velocity models, was reduced to 0.057 s. The rms distribution, before and after the 3D inversion, is shown in Fig. 14.

The resulting V_P and V_P/V_S models described the geological and tectonic regime of the area very well. The most obvious features are the Rio graben and the Antirio fault zone in the

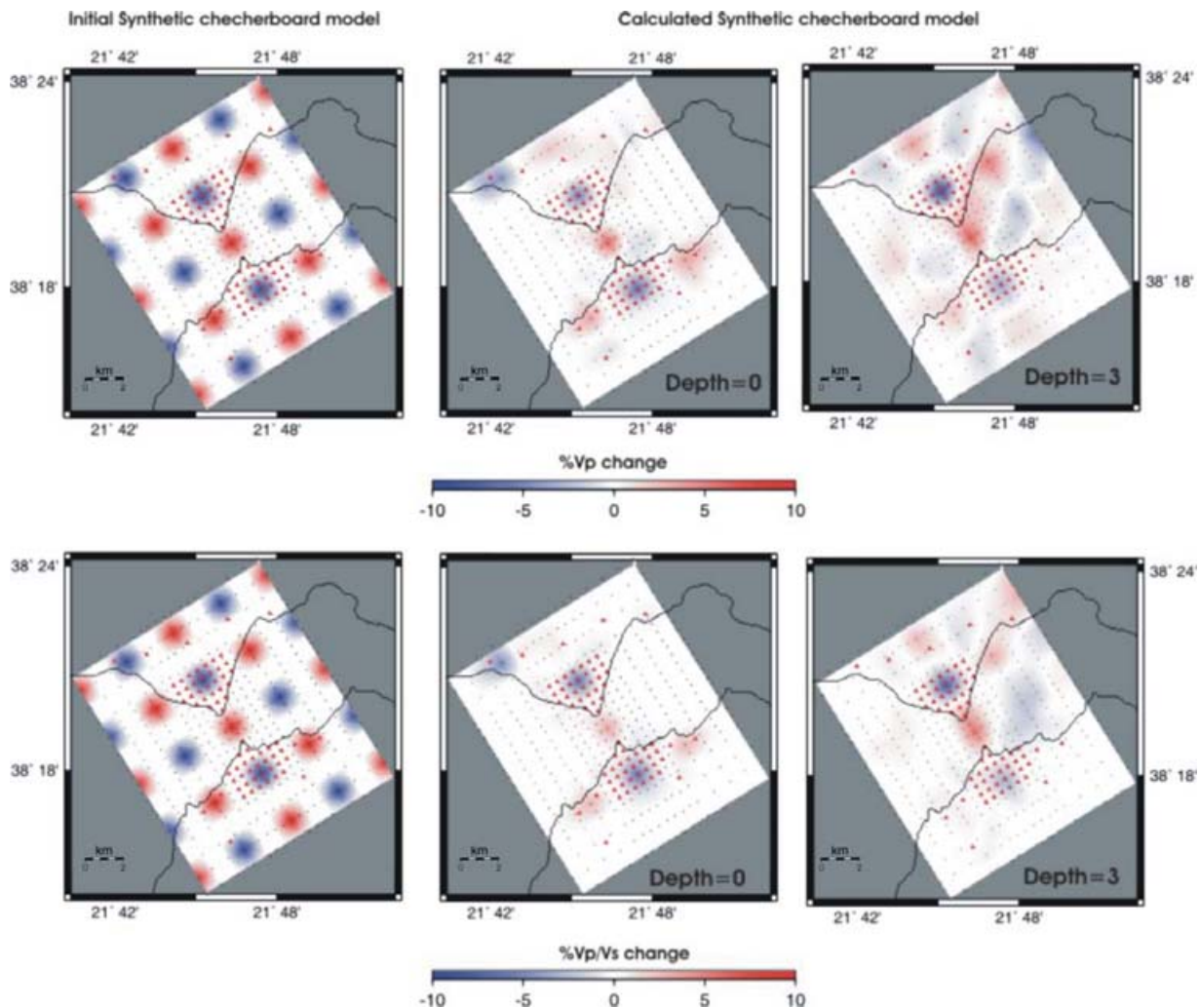


Figure 17 Checkerboard test for V_P model (top) and V_P/V_S model (bottom). The velocity anomalies within the target area are very well recovered.

northern part of the network (Fig. 15). Figures 15(a,b) shows characteristic cross-sections of V_P and V_P/V_S and Fig. 15c shows a 3D view of the resultant V_P model. V_P values of less than 3 km/s and V_P/V_S values of more than 1.9 correspond to Quaternary and Neogene formations. The thickness of these formations at the target area is approximately 500–600 m (Figs 15a,b). Previous geological studies in the area (Kontopoulos and Doutsos 1985) agree with the passive seismic estimation. Also, shallow drillings (down to 100 m below the sea bottom) for the construction of the Rio-Antirio Bridge concurred with these results, indicating the presence of Quaternary formations (i.e. sand and gravel, clay, silt). P-wave velocities greater than 5.2 km/s and V_P/V_S values of 1.8 characterize the alpine basement.

Figure 16 shows plan views of V_P and V_P/V_S models at 0 and 3 km depth. Following the same resolution analysis procedure described in the previous case study, we show (Figs 17,18 and 19) the checkerboard tests and the hit count, DWS and RDE or V_P and V_P/V_S models. Based on these tests, areas with hit count, DWS and RDE values of more than 200, 1500 and 0.2, respectively, are considered as the best resolved.

At the area of interest, where the seismic network is very dense, the ray coverage and the recovery of synthetic velocity anomalies are very good near the surface, as well as at 3 km depth (especially for the V_P model because of the significantly larger number of P-wave arrivals). Although the resolving power of data was reduced in the offshore part of the model due to the ‘network gap’, the successful recovery

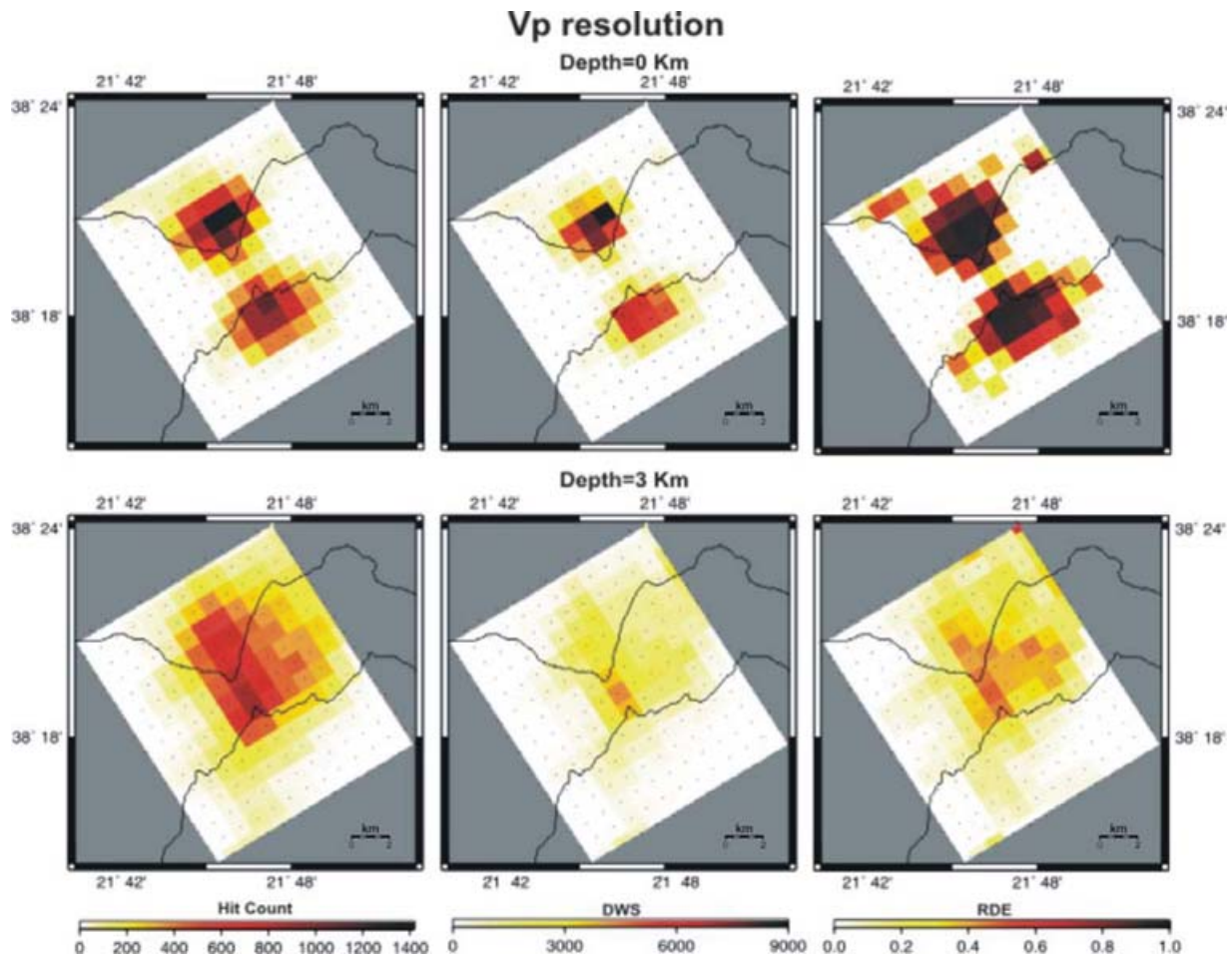


Figure 18 Description of resolution parameters at 0 km (top) and 3 km depth (bottom) for P-wave velocity model.

of the velocity anomaly indicates that by adopting a graded inversion scheme, we were able to provide a reliable velocity model. At the periphery of the target area, some of the velocity anomalies are recovered but they present some smearing due to sparseness of the seismic network.

CONCLUSIONS

Designing a passive seismic survey is more complicated than simply deploying seismographs over the area to be investigated. To get the best resolution of the geological formations at the lowest cost, geophysicists are tapping an arsenal of technology, from initial velocity model selection to simultaneous earthquake hypocentre and 3D velocity model inversion, and synthetic and real data checkerboard tests. The depicted examples prove that this new technology can be a valuable tool for earthquake prediction surveys and hydrocarbon exploration, especially in the case of large areas or areas characterized by

difficult geological regimes (thrust belts, seismic penetration problems, difficult topography, etc.). In hydrocarbon exploration, passive seismic can be used as reconnaissance tool in order to optimize the cost of 3D conventional seismic surveys. It can also be used as a complementary method for the reinterpretation of 2D regional seismic data, reprocessing of 2D seismic data using the velocity model derived by passive seismic, and defining new target areas that are not visible in 2D or other geophysical data.

ACKNOWLEDGEMENTS

The authors and LandTech Enterprises thank Enterprise Oil and partners and the Railway Organization of Greece for permission to publish the results of the case studies. We also thank Dr A. Serpetsidaki, Dr E. Sokos and Mr A. Sotiriou from the Seismological Laboratory of Patras University,

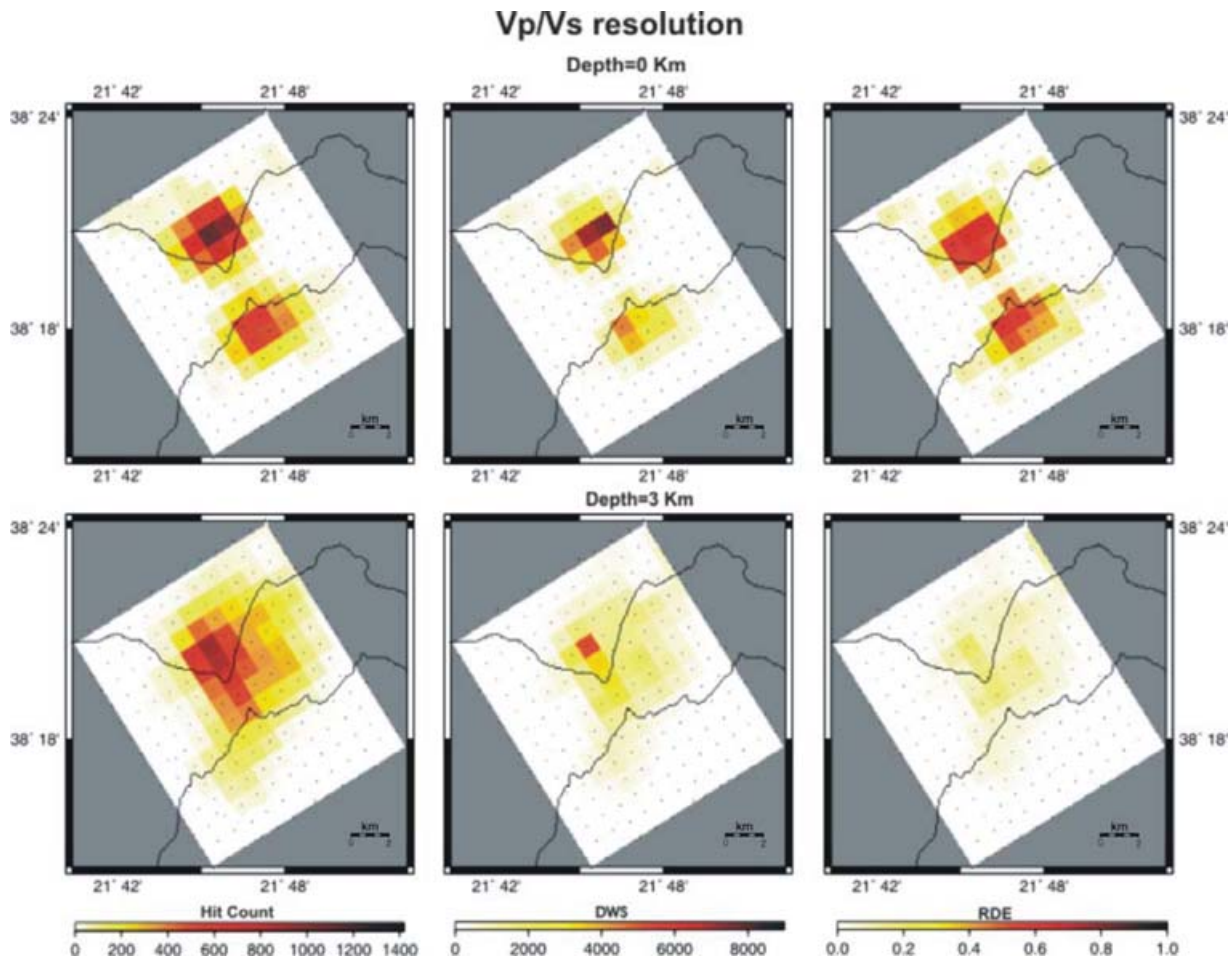


Figure 19 Description of resolution parameters at 0 km (top) and 3 km depth (bottom) for V_p/V_s model.

Dr N. Xanalatos and Mrs M. Sarris for their contributions to this study.

REFERENCES

- Eberhart-Phillips D. 1986. Three-dimensional velocity structure in northern California Coast Ranges, for inversion of local arrival times. *Bulletin Seismological Society America* 76, 1025–1052.
- Evans J.R., Eberhart-Phillips D. and Thurber C.H. 1994. User's manual for SIMULPS12 for imaging V_p and V_p/V_s : A derivative of the 'Thurber' tomographic inversion SIMUL3 for Local Earthquakes and Explosions. U.S. Geological Survey, Open File Report, 94–431.
- Haslinger F. 1998. Velocity structure, seismicity and seismotectonics of Northwestern Greece between the Gulf of Arta and Zakynthos. PhD Thesis, Swiss Federal Institute of Technology, Zurich.
- Kapotas S., Tselentis G. and -Akis and Martakis N. 2003. Case study in NW Greece of passive seismic tomography: a new tool for hydrocarbon exploration. *First Break* 21, 37–42.
- Klein F. 2002. User's guide to Hypoinverse-2000a fortran program to solve for earthquake locations and magnitudes. US Geological Survey, Open File Report, 02–171.
- Kontopoulos N. and Doutsos T. 1985. Sedimentology and tectonic of the Antirion area (Western Greece). *Bollettino della Societa Geologica Italiana* 104, 479–489.
- Lanczos C. 1961. *Linear Differential Operators*. Van Nostrand, London.
- Lee W.H.K. and Lahr J.C. 1972. HYPO71 (revised): A computer program for determining hypocenters, magnitude and first motion pattern of local earthquakes. U.S. Geological Survey, Open File Report, 75–311.
- Lee W.H.K. and Stewart S.W. 1981. *Principals and Applications of Microearthquake Networks*. Academic Press, Inc.
- Melis N.S. and Tselentis G.-A. 1998. 3-D P-wave velocity structure in Western Greece determined from tomography using earthquake data recorded at the University of Patras seismic network (PATNET). *Pure and Applied Geophysics* 152, 329–348.
- Michellini A. and McEvilly T.V. 1991. Seismological studies at Parkfield. Simultaneous inversion for velocity structure and hypocenters

- using cubic B-splines parameterization. *Bulletin Seismological Society America* **81**, 524–552.
- Thurber C.H. 1983. Earthquake locations and three-dimensional crustal structure in Coyote Lake area, Central California. *Journal of Geophysical Research* **88**, 8226–8236.
- Toomey D.R. and Fougler G.R. 1989. Tomographic inversion of local earthquake data from the Hengill-Grensdalur central volcano complex. *Iceland. Journal of Geophysical Research* **94**, 17497–17510.
- Waldhauser F. 2001. HypoDD-A program to compute double difference hypocenter locations. US Geological Survey, Open File Report, 01–113.
- Xanlatos N. and Tselentis G.-A. 1997. SEISMWIN, an algorithm for processing seismological waveforms. *Proceedings of the Geological Society Athens* **22**, 235–246.